Article

Cuttlefish bone-derived biphasic calcium phosphate scaffolds coated with sol-gel derived bioactive glass

Ana S. Neto, Daniela Brazete, José M.F. Ferreira *

Department of Materials and Ceramic Engineering, CICECO, University of Aveiro, 3810-193 Aveiro, Portugal
* Corresponding author: jmf@ua.pt; Tel.: +351-234-370-242

Abstract: The combination of calcium phosphates (CaP) with bioactive glasses (BG) has received an increased interest in the field of bone tissue engineering. In the present work, biphasic calcium phosphates (BCP) obtained by hydrothermal transformation (HT) of cuttlefish bone (CB) were coated with a Sr-, Mg- and Zn-doped sol-gel derived BG. The scaffolds were characterized by X-ray diffraction (XRD), Fourier transform infrared spectroscopy (FTIR) and scanning electron microscopy (SEM). The initial CB structure was maintained after HT and the scaffold functionalization did not jeopardize the internal structure. The results of in vitro bio-mineralization after immersing the BG coated scaffolds in simulated body fluid (SBF) showed extensive formation of bone-like apatite onto the surface of the scaffolds. Overall, the functionalized CB derived BCP scaffolds revealed promising properties for their use in bone tissue engineering field.

Keywords: Cuttlefish bone; Biphasic calcium phosphate; Porous scaffolds; Sol-gel coatings; Bioactivity; Tissue engineering

1. Introduction

Bone is the second most transplanted tissue after blood. Autologous bone grafts are still considered the gold standard procedure, but unfortunately, their availability is limited and they are intimately associated with donor site morbidity [1]. Thus, bone tissue engineering represents an important challenge in order to overcome the shortcomings of bone grafts, where porous scaffolds can be combined with cells and bioactive growth factors, providing a suitable environment for tissue development [2]. Bioceramic-based scaffolds have been successfully used for bone repair and replacement. Among the different bioceramics, calcium phosphate materials (CaP) like hydroxyapatite (HA) and β-tricalcium phosphate (β-TCP) are the most commonly used ones due to their close chemical similarity to the inorganic part of the bone. HA is stable under physiological conditions and has a slow resorption rate and; on the other hand, β-TCP is a more soluble phase with a lower mechanical stability. Mixtures of HA and β-TCP phases originate biphasic calcium phosphate (BCP) materials and enable to control the bioactivity and the balance between resorption and solubilisation rates [3]. Bioactive glasses (BGs) have been used as an alternative to CaP materials. They have the capacity to strongly bond to the living tissues, through the growth of a bone-like HA layer on the glass surface [4,5]. Moreover, BGs release critical concentrations of ions like Si, P or Ca, which act as chemical stimuli for the activation of osteoprogenitor cells and, consequently, enhance bone formation. The release of these ions is also known to stimulate neovascularisation and angiogenesis and, thereby, promoting bone healing [6,7]. BGs were firstly synthesized by melt-quenching technique. Nevertheless, the sol-gel approach has been gaining more relevance in the last decades [8–10]. When compared to melt-quenching, the sol-gel derived BGs are prepared at significantly lower temperatures and they have a higher specific surface area, which, consequently, enhances their bioactive response [11]. Apart from that, the sol-gel derived BGs can be prepared with amounts of SiO_2 up to 90 wt.%, whilst SiO_2 contents higher than 60 wt.% are hardly achievable by melt-quenching [12]. The high number of Si–OH groups in sol-gel derived BG is beneficial for a further functionalization [13]. Moreover, the composition of sol-gel derived BG can be more easily tailored to achieve the desired physicochemical and biological properties. Under this regard, the

incorporation of metal ions in the silicate network have been widely investigated [14–18]. The incorporation of strontium (Sr) into the BGs enhances bone formation as it promotes osteoblast differentiation and simultaneously inhibits osteoclast differentiation. In addition, in vivo studies demonstrated that the Sr–doped BGs strongly bond to the bone through the apatite layer [19,20]. The incorporation of magnesium (Mg) into BGs improves the dissolution behaviour as it promotes the disruption of the silica network [21]. Furthermore, Mg–doped BGs promote osteoblast proliferation and differentiation [22]. On the other hand, the introduction of zinc (Zn) into BGs favours osteoblast proliferation and differentiation [16]. Additionally, Zn demonstrated to exert anti-inflammatory effects [23].

The combination of CaP with bioactive glasses (BG) has received an increased interest in the bone tissue engineering field, since it develops a synergetic effect improving the properties of the bone graft materials [24,25]. It was demonstrated that the incorporation of BG into a CaP material enhances the mechanical strength through the densification of the material. In addition, the bioactivity of CaP is lower when compared to those of BGs. Thereby, a combination of these types of materials originates bone grafts with enhanced biological responses [26].

This work aims at developing BG-coated BCP scaffolds, taking advantages of their synergetic effect. BCP scaffolds obtained through the hydrothermal transformation (HT) of cuttlefish bone (CB) were coated with a Sr-, Mg- and Zn-doped sol-gel derived BG (60% SiO2 – 34% CaO – 2% SrO – 2% MgO – 2% ZnO – 2% P2O5 (mol%), and the bio-mineralization activities of uncoated and BG-coated scaffolds were tested in vitro in simulated body fluid.

2. Materials and Methods

2.1. Preparation of BCP scaffolds

BCP scaffolds were obtained through HT of the hard aragonite porous structure of cuttlefish (Sepia officinalis). Firstly, the exact amount of $CaCO_3$ present in CB sample was determined by differential thermal and gravimetric thermal analyses (DTA/TG, Labsys Setaram TG-DTA/DSC, France, heating rate 10 °C min^{-1}). According to the obtained result, CB was cut into small pieces and it was added the required volume of the phosphorous precursor solution, di-ammonium hydrogen phosphate [$(NH_4)_2HPO_4$, Panreac AppliChem, Spain]. Subsequently, the as-prepared mixtures were sealed in poly(tetrafluorethylene) lined stainless steel autoclave. The reaction took place at 200 °C for 24 h in the over. The as-obtained scaffolds were subjected to a heat treatment at 700 °C for 1 h and using a heating rate of 0.5 °C min^{-1} to burn the organic material followed by a sintering at 1200 °C using a and heating rate of 2 °C min^{-1} and a dwelling time of 2 h.

2.2. Preparation of sol-gel derived BG and coating of the BCP scaffolds

In this study it was used a sol-gel derived BG with the composition of 60% SiO_2 – 34% CaO – 2% SrO – 2% MgO – 2% ZnO – 2% P_2O_5 (mol%). To prepare the BG, tetra-ethyl-ortho-silicate (TEOS, $C_8H_{20}O_4Si$, Sigma–Aldrich, Germany) and triethyl phosphate (TEP, $C_6H_{15}O_4P$, Sigma–Aldrich, Germany) were mixed in 10 mL of water. The pH was adjusted to values between 1 and 2, using nitric acid (HNO_3, Panreac AppliChem, Spain) and mixed for 1 h. Calcium nitrate tetrahydrate [$Ca(NO_3)_2·4H_2O$, Panreac AppliChem, Spain] was used as the precursor of calcium. Furthermore, strontium nitrate, $Sr(NO_3)_2$, Magnesium nitrate hexahydrate, $Mg(NO_3)_2·6H_2O$, and zinc nitrate hexahydrate, $Zn(NO_3)_2·6H_2O$, all from Sigma-Aldrich, Germany, were used as the precursors of strontium, magnesium and zinc. These nitrate salts were dissolved in 10 mL of water and, subsequently, added to the first solution and kept under magnetic agitation for 1 h to obtain a homogenous solution. The as-obtained sol was used for the coating of the BCP scaffolds. For this purpose, the scaffolds were immersed in the BG sol and placed in the vacuum chamber under a pressure of 0.4 bar for 20 min. Subsequently, the impregnated scaffolds were placed in an oven at 100 °C for 24 h. The scaffolds were sintered at 700 °C for 2 h and with a heating rate of 0.3 °C min^{-1}.

2.3. Sample Characterization

2.3.1. X-ray diffraction

X-ray diffraction (XRD) was used to identify the crystalline phases of the BCP scaffolds derived from CB as well as to confirm the glass state of the synthesized sol-gel derived BG. The data were collected in 2θ range between 10º and 100º with a 2θ–step size of 0.0260º per second in a High Resolution X-ray Diffractometer (PANalytical X'Pert PRO) with Cu Kα radiation (λ = 1.5406 Å) produced at 40 mA and 45 kV. The relative percentages of the crystalline phases were estimated by using the HighScorePlus, a spectra-fitting software.

2.3.2. Fourier transform infrared

The sol-gel derived BG as well as the uncoated and coated scaffolds were examined by attenuated total reflection Fourier transform infrared spectroscopy (FTIR-ATR). Data were collected over the spectral range of 400–4000 cm⁻¹ with a total of 256 scans and a spectral resolution of 4 cm⁻¹ in a FTIR Bruker Tensor 27 equipped with a Golden Gate Single Reflection Diamond ATR.

2.3.3. Dilatometry

The sintered uncoated scaffolds and the dried BG were grinded and powdered. From the obtained powder it was prepared cylindrical rods with a diameter of 4.50 mm and a length of approximately 10 mm were used for dilatometry measurements (Bahr Termo Analyse DIL 801 L, Hiillhorst, Germany; heating rate of 5 ºC min–1). The thermal expansion coefficient was obtained according to Eq. (1),

$$\alpha = \frac{1}{L_0}\left(\frac{\triangle L}{\triangle T}\right) \qquad (1)$$

Here, α is the thermal expansion coefficient, L0 is the initial sample length, Δ L is the change in length and Δ T is the change in temperature.

2.3.4. Microstructure

Micro computed tomography (μ-CT, Bruker) was used to observe the interconnectivity of raw CB microstructure. It was used an exposure time of 800 ms, energy of 50 kV and intensity of 200 μA. The NRecon software was used for the reconstruction of cross-section images. The microstructure of the samples was also observed by scanning electron microscopy (SEM, Hitachi SU-70, Hitachi High-Technologies Europe, GmbH, Germany) using an acceleration voltage of 15 kV. The samples were coated with carbon. Energy dispersive spectroscopy (EDS) was used to examine the presence of the doping elements in the samples.

2.3.5. Mechanical properties

The uncoated and coated cubic shape scaffolds with approximately 3 mm side were subjected to a uniaxial compressive strength by using a universal testing machine (AG-IS10kN, Shimadzu, Kyoto, Japan). The samples were subjected to a maximum load of 200 N and it was used a constant crosshead speed of 0.5 mm min⁻¹ in ambient conditions. The compressive load was applied perpendicularly to the lamella of BCP scaffolds derived from CB.

2.4. In-vitro bio-mineralization

The uncoated and coated scaffolds were immersed in simulated body fluid (SBF) solution with an ionic concentration similar to those of human blood plasma to evaluate the in vitro scaffold's bioactivity. For this purpose, the immersed samples were placed in an orbital shaker at 37 °C for 14 days. The SBF solution was prepared accordingly to the international standard ISO 23317 but while using a unified standard area of 0.5 cm² mL⁻¹ proposed elsewhere [27]. After each immersion period, the samples were removed from SBF solution, rinsed with distilled water and then left to dry in a

silica desiccator. Once dried, the morphology of the scaffolds was analysed by SEM to observe the bioactive layer deposited onto their surfaces.

2.5. Statistical analysis

The experiments were performed in triplicated and the values are expressed as mean ± standard deviation (SD). The statistical analysis was performed using a Student's t-test. $P < 0.05$ was considered statistically significant.

3. Results

3.1. Chemical and structural characterization

Figure 1 displays the XRD patterns of the sol-gel derived BG as well as the ones regarding the scaffolds before and after coated with BG by immersion in the sol, followed by heat treatment at 700 °C for 2 h. The sol-gel derived BG exhibited essentially an amorphous character. On the other hand, the scaffolds before and after the impregnation with BG, followed by heat treatment at 700 °C for 2 h, exhibited similar patterns, with HA (# 04-015-7245) and β-TCP (# 04-006-9376) being the identified crystalline phases. As estimated by HighScorePlus software, the relative percentages of crystalline phases presented in the scaffolds were 63.9% HA and 36.1% β-TCP before the BG coating and 64.6% HA and 35.4% β-TCP after the BG coating.
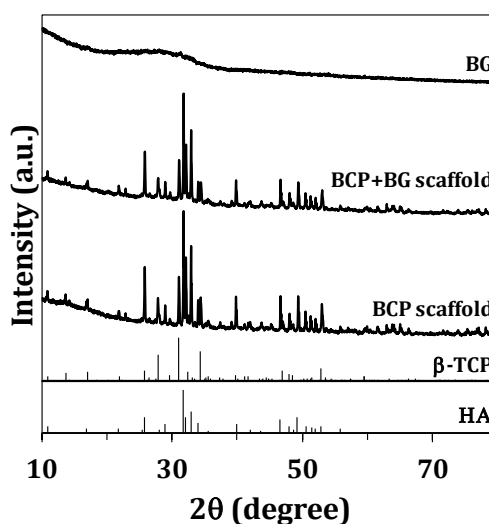

Figure 1. Sol-gel derived BG, BCP scaffolds and BG-coated scaffolds. The standard diffraction patterns of β-TCP and HA standards, ICDD PDF 04-006-9376 and 04-015-7245, respectively, are also present for comparison purposes.

The FTIR spectra of the sol-gel derived BG and the BCP scaffolds before and after the coating with BG are shown in Figure 2. The FTIR spectra of sol-gel derived BG exhibit a characteristic broad band for the asymmetric stretching for Si–O–Si from 900 and 1300 cm^{-1} and centred at 1080 cm^{-1}. The peak at 800 cm^{-1} is also assigned to the stretching mode of Si–O–Si [28]. Moreover, the FTIR spectra of the uncoated and coated scaffolds are identical and exhibit the characteristic vibrational modes of –PO$_4$ and –OH groups. The band present at 470 cm^{-1} denotes the ν2 mode of O–P–O bending, while the ν4 mode of O–P–O bending is present at 550 and 600 cm^{-1}. The band at 960 cm^{-1} is associated with ν1 P–O stretching mode. The bands located at 1000 and 1088 cm^{-1} are due to the ν3 mode. The bands at 940 and 960 cm^{-1} denote the ν1 non-degenerate P–O symmetry stretching mode. The vibrational mode of –OH group appear at 630 cm^{-1} with low intensity and the stretching mode should appear at 3575 cm^{-1} [29].
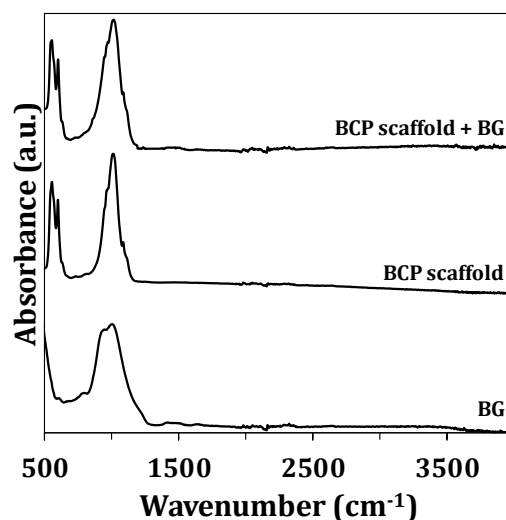
Figure 2. FTIR spectra of sol-gel derived BG, BCP scaffolds and BG-coated scaffolds.

3.2. Microstructure

The unique layered and interconnected porosity of CB was observed by μ-CT (Figure 3a). The porous architecture of scaffolds after HT and sintering processing steps, and also after BG coating and calcination, was analysed by SEM. From the images displayed in Figure 3b, one can observe that the internal structure of CB was preserved after HT and sintering.
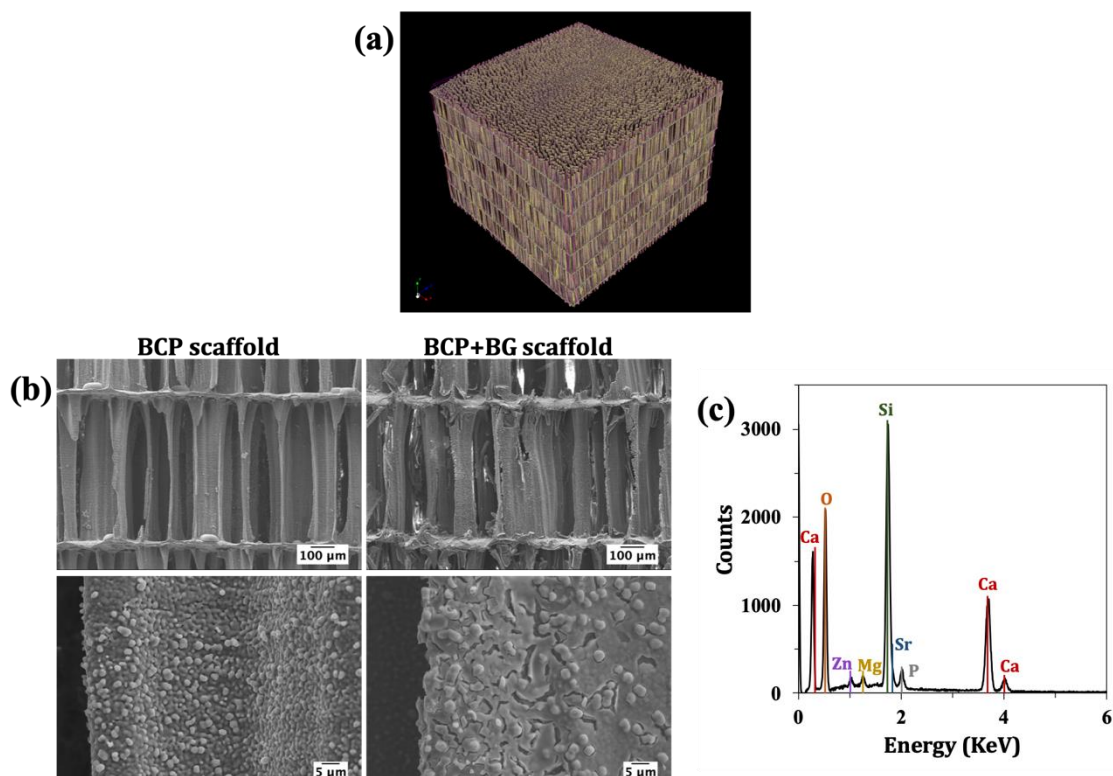

Figure 3. Microstructural and chemical features of the scaffolds: **(a)** μ-CT image showing the microstructure of raw CB highlighting its interconnected porosity; **(b)** SEM micrographs of uncoated and coated BCP scaffolds; **(c)** EDS analysis of the sol-gel derived BG coating.

Moreover, the sintering step promoted the development of grains. The BCP scaffolds were successfully coated with BG and the presence of the doping elements was confirmed by the results of EDS analysis shown in Figure 3c. The amounts of strontium, magnesium and zinc were 1.77, 2.07

and 1.11 mol%. The measured values for Sr, and Mg are comparable to the planned contents (2 mol%), while for Zn only ~55% of the planned amount has been effectively incorporated. Moreover, coating with the sol-gel derived BG did not obstruct the pores. The surface coating presents some cracks, which can be attributed to the high retraction extents that are typically observed for sol-gel derived BG during the dry and calcination steps. The coefficient of thermal expansion of the BG coating material was 2.27×10^{-6} °C^{-1}, while that measured for the BCP scaffold derived from CB was 8.15×10^{-6} °C^{-1} (i.e., about 3.6 times higher). However, the cracks observed in the sol-gel coatings are much less attributable to this difference in the coefficients of thermal expansion, but more to the extent of shrinkage undergone by the coating especially under the drying step.

3.3. Mechanical properties

The characteristic stress-strain curves are displayed in Figure 4a. It can be seen that both uncoated and coated scaffolds undergo a gradual collapse layer-by-layer. The average compressive strengths of uncoated and coated scaffolds were calculated from the maxima mechanical stress values measured during deformation. The results plotted in Figure 4b show that the average compressive strength of BCP scaffolds derived from CB was 0.26 ± 0.02 MPa, while a higher value of 0.36 ± 0.04 MPa was registered for BG-coated scaffolds. This means that the BG coating significantly improves the mechanical performance of the BCP scaffolds.
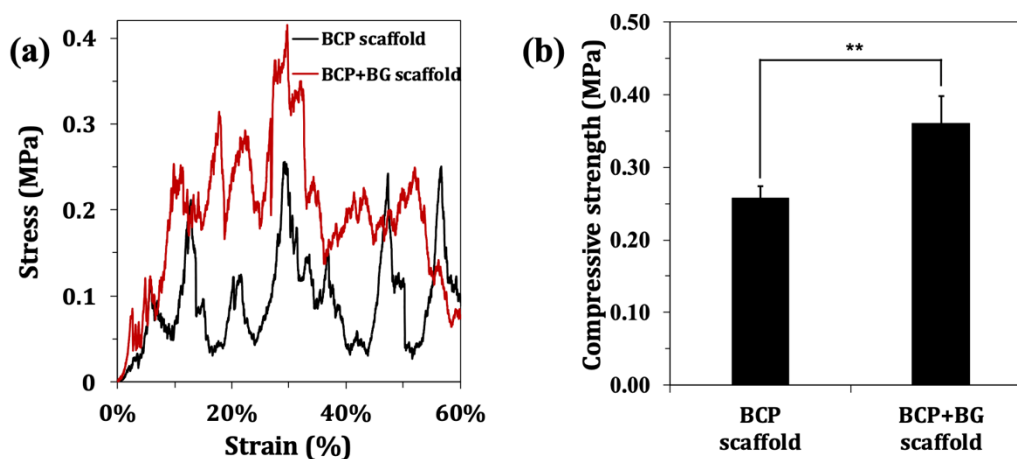

Figure 4. Compressive strength of uncoated and BG-coated BCP scaffolds: **(a)** representative stress-strain curve; **(b)** maximum mechanical stress during the deformation period. Results are represented as mean ± SD (*P < 0.05 and **P < 0.05)

3.4. In-vitro bio-mineralization

The material capacity to bond the natural bone upon implantation is normally evaluated by immersion in SBF solution, which is recognized to be an interesting first approach to predicting the bioactivity of a material [30]. Figure 5 shows the SEM micrographs of the scaffolds after 14 days of immersion in SBF solution. After this immersion period, the roughness of the coated scaffolds significantly increased in comparison to the that of uncoated samples. Therefore, the BG coating also improves the in-vitro bio-mineralization ability of the scaffolds. These results can be explained considering that the calcium phosphate materials like hydroxyapatite are more chemically stable under pH conditions similar to those existing in the physiological fluid in comparison to BG [3]. This, combined with the ability to form a bone-like HA layer confer to bioactive glasses their capacity to strongly bond to the living tissues [4,5].
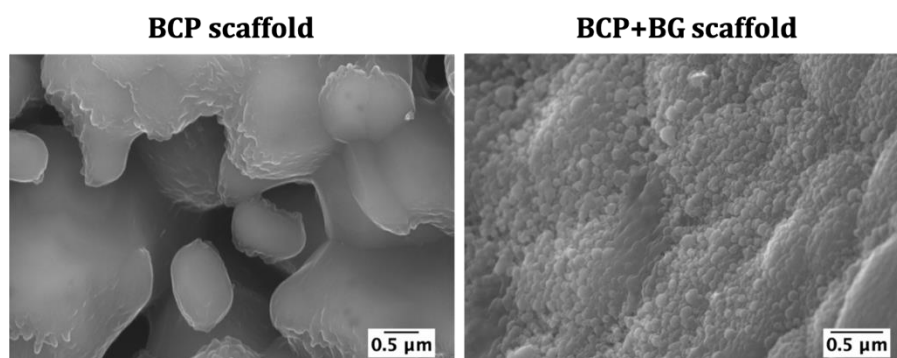
BCP scaffold   **BCP+BG scaffold**

Figure 5. SEM micrographs of uncoated and BG-coated BCP scaffolds after 14 days of immersion in SBF solution.

4. Discussion

A Sr-, Mg- and Zn-doped sol-gel derived BG was prepared and used to coat BCP scaffolds derived from CB. The amorphous nature of sol-gel derived BG was demonstrated by XRD (Figure 1) and also confirmed by the FTIR pattern (Figure 2), showing the characteristic Si–O bands. The absence of any calcium carbonate phase in the scaffolds after the HT transformation and the only presence of XRD patterns characteristic of HA and β-TCP peaks, prove that the original aragonite was for the first time successfully and completely transformed into BCP scaffolds. This is a novel and very important achievement, since any untransformed calcium carbonate will decompose during the subsequent sintering step, leading to the formation of free CaO. The free CaO, in turn, tends to react with body fluid to form $Ca(OH)_2$, therefore creating a cytotoxic alkaline environment after implantation in vivo. Moreover, and in agreement with the previous results, the FTIR spectrum of BCP scaffold demonstrated the presence of $-PO_4$ and $-OH$ groups. Nonetheless, $-OH$ groups are mainly inexistence due to their absence in β-TCP phase and the partial de-hydroxylation of HA upon sintering at 1200 °C. After BG coating the scaffolds with BG, the XRD pattern remains unchanged, indicating that the surface coating remains amorphous and is fine enough for do not hidden the BCP nature of the substrate. With respect to the FTIR spectra, the characteristic Si–O band located between 900 and 1300 cm^{-1} appeared overlapped with $-PO4$ bands, making difficult to distinguish the differences between uncoated and coated scaffolds.

The μ-CT image of CB (Figure 3a) demonstrated the unique structural features of CB, which are known to be beneficial for bone development [31]. The unique microstructure was preserved after the HT and sintering steps (Figure 3b). Moreover, it is important to highlight that after the BG coating the interconnected porous structure was not compromised (Figure 3b). Through EDS analysis (Figure 3c) was possible to observe that the doping elements Sr and Mg were present in the coating layer in amounts that are close to the planned ones. The incorporation extent of Zn was only ~55%. This lower efficiency of zinc for entering in the glass silicate network as doping element may be related to its less marked network-modifying role in comparison to the alkaline earth elements. It was found recently that Zn^{2+} tends to adopt a mixed tetrahedral and octahedral coordination in the glassy network and copolymerizes with [SiO4] tetrahedra [32]. On average, a Zn^{2+} was coordinated with ~4.9 non-bridging oxygens (NBOs), a lower value in comparison to the alkaline earth elements (~5.9 NBOs for Ca^{2+}, and 5.1 NBOs for Mg^{2+}). The lower coordination number of Zn^{2+} suggests that it is probably closer to an intermediate role, reflecting its higher field strength with respect to alkaline earth ions.

Apart from that, the BG coating layer exhibited some cracks because of the sol-gel drying and sintering processes. Despite the observed difference between the thermal expansion coefficients of BCP scaffolds ($8.15 \times 10{-6}$ °C^{-1}) and BG coating ($2.27 \times 10{-6}$ °C^{-1}), the cracks observed in the SEM images of the coated scaffolds cannot be attributed to this difference. In fact, a coating with a lower coefficient of thermal expansion will undergo smaller dimensional changes upon cooling from the heat treatment temperature (700 °C) to room temperature in comparison to those experienced by the substrate. Therefore, these cracks are only due to the considerable shrinkage undergone by the sol-gel coating during the subsequent heat treatment schedules, especially upon drying step.

Despite the fine thickness of the BG coating, the mechanical properties of the scaffolds improved in a significant way as seen in Figure 4. However, the compressive strength of the coated scaffolds (0.36 ± 0.04 MPa) are within the lower range of the compressive strength of trabecular bone that varies between 0.1 and 16 MPa [33]. This result could be associated with the 92% porosity of the scaffolds. However, this seems not to be a problem, as the scaffolds are thought essentially as bone graft filers, therefore not subjected to significant load bearing conditions. Even through, the mechanical properties could be further improved by applying successive thinner sol-gel derived BG coatings.

The scaffolds exhibited a good in vitro bio-mineralization activity, reflected by the increases in surface roughness after the immersion period of 14 days in SBF, as can be observed in Figure 5. The less remarkable surface changes that occurred for the uncoated scaffolds can be attributed to their higher chemical stability under pH values similar to that of physiological fluid [3]. Oppositely, bioactive glasses have the ability to release other ionic species that may contribute to oversaturate the SBF solution, inducing the surface dissolution-precipitation reactions [4,5]. Besides this advantages, the various ionic species release from the BG-coating may activate the osteoprogenitor cells and stimulate the biological processes (neovascularisation and angiogenesis) necessary for promoting bone healing [6,7].

More extensive and remarkable surface changes are likely to occur during longer times of immersion in SBF. The scaffolds are promising for being further in vitro investigated in cell cultures. These investigations are still underway and will be reported in a near future.

Overall, the surface functionalization of the BCP scaffolds with a sol-gel derived BG enabled to obtain materials with higher bioactivity and compressive strength, and with the ability to release ionic species (Sr^{2+}, Mg^{2+} and Zn^{2+}) that are known to be beneficial for bone development.

5. Conclusions

In the present study, porous BCP scaffolds derived from aragonite CB and with the complete absence of any calcium carbonate phase were, for the first time, successfully prepared by HT transformation. This is a novel and very important achievement, since any untransformed calcium carbonate will decompose during the subsequent sintering step, leading to the formation of free CaO. The free CaO, in turn, tends to react with body fluid to form $Ca(OH)_2$, therefore creating a cytotoxic alkaline environment after implantation in vivo. The BCP scaffolds consisting of 63.9 % HA and 36.1 % β-TCP BCP were coated with a Sr-, Mg- and Zn-doped sol-gel derived BG, which enhanced their bio-mineralization activity in SBF and compressive strength, enabling to accomplish the aimed targets. The BG coating was completely amorphous and the incorporation levels of doping alkaline earth ions (Sr^{2+}, Mg^{2+}) did not differ much from the planned ones, while the incorporation level of Zn^{2+} was noticeably lower (only ~55% relative to the planned one). The unique porous microstructure of raw CB was neither damaged during the HT and sintering steps, nor compromised after the BG coating. The micro-cracked appearance of the sol-gel derived BG coating is solely due to the shrinkages undergone during the drying and sintering processes. In summary, the porous BCP scaffolds surface functionalized with the sol-gel derived BG coating seem very promising for being further investigated as bone graft materials and constructs for bone tissue engineering.

Author Contributions: All the authors have contributed to this research article. J.M.F.F. conceived and designed the main structure of the article and, together with D.B. did the specific literature survey and analysis about sol-gel derived bioactive glasses. D.B. also did the first exploratory experiments on the sol-gel synthesis and characterization of bioactive glasses. A.S.N. is a PhD student doing research on synthetic bone graft substitutes based on calcium phosphates and on the use of CB for biomedical applications. Her PhD work programme, conceived and designed by J.M.F.F., aims at developing porous scaffolds by the hydrothermal transformation of CB into biphasic calcium phosphates while preserving its unique porous structure. A.S.N. was in charge of performing most of the literature survey and analysis, and of elaborating the first draft of the parts more closely related to her PhD work programme, as well of integrating the spare contributes received from the other authors into a single document. The supervisor conducted the final check of and provided refinements to the entire document.

Conflicts of Interest: The authors declare no conflicts of interest.

References

1.   Sen, M. K.; Miclau, T. Autologous iliac crest bone graft: should it still be the gold standard for treating nonunions? *Injury* **2007**, *38 Suppl 1*, S75–S80, doi:10.1016/j.injury.2007.02.012.

2.   O'Brien, F. J. Biomaterials & scaffolds for tissue engineering. *Mater. Today* **2011**, *14*, 88–95, doi:10.1016/S1369-7021(11)70058-X.

3.   Bouler, J. M.; Pilet, P.; Gauthier, O.; Verron, E. Biphasic calcium phosphate ceramics for bone reconstruction: A review of biological response. *Acta Biomater.* **2017**, *53*, 1–12, doi:10.1016/j.actbio.2017.01.076.

4.   Cao, W.; Hench, L. L. Bioactive Materials. *Ceram. Int.* **1996**, *22*, 493–507, doi:10.1016/0272-8842(95)00126-3.

5.   Hench, L. L.; Splinter, R. J.; Allen, W. C.; Greenlee, T. K. Bonding mechanisms at the interface of ceramic prosthetic materials. *J. Biomed. Mater. Res.* **1971**, *5*, 117–141, doi:10.1002/jbm.820050611.

6.   Jones, J. R. Reprint of: Review of bioactive glass: From Hench to hybrids. *Acta Biomater.* **2015**, *23*, S53–S82, doi:10.1016/j.actbio.2015.07.019.

7.   Hoppe, A.; Güldal, N. S.; Boccaccini, A. R. A review of the biological response to ionic dissolution products from bioactive glasses and glass-ceramics. *Biomaterials* **2011**, *32*, 2757–2774, doi:10.1016/j.biomaterials.2011.01.004.

8.   Fiume, E.; Barberi, J.; Verné, E.; Baino, F. Bioactive glasses: From parent 45S5 Composition to Scaffold-Assisted Tissue-Healing Therapies. *J. Funct. Biomater.* **2018**, *9*, 24, doi:10.3390/jfb9010024.

9.   Baino, F.; Fiume, E.; Miola, M.; Verné, E. Bioactive sol-gel glasses: Processing, properties, and applications. *Int. J. Appl. Ceram. Technol.* **2018**, *15*, 841–860, doi:10.1111/ijac.12873.

10.   Kaur, G.; Pickrell, G.; Sriranganathan, N.; Kumar, V.; Homa, D. Review and the state of the art: Sol-gel and melt quenched bioactive glasses for tissue engineering. *J. Biomed. Mater. Res. Part B Appl. Biomater.* **2016**, *104B*, 1248–1275, doi:10.1002/jbm.b.33443.

11.   Zhong, J.; Greenspan, D. C. Processing and properties of sol-gel bioactive glasses. *J. Biomed. Mater. Res.* **2000**, *53*, 694–701, doi:10.1002/1097-4636(2000)53:6<694::AID-JBM12>3.0.CO;2-6.

12.   Li, R.; Clark, A. E.; Hench, L. L. An Investigation of Bioactive Glass Powders by Sol-Gel Processing. *J. Appl. Biomater.* **1991**, *2*, 231–239, doi:10.16953/deusbed.74839.

13.   Treccani, L.; Yvonne Klein, T.; Meder, F.; Pardun, K.; Rezwan, K. Functionalized ceramics for biomedical, biotechnological and environmental applications. *Acta Biomater.* **2013**, *9*, 7115–7150, doi:10.1016/j.actbio.2013.03.036.

14.   Lázaro, G. S.; Santos, S. C.; Resende, C. X.; Dos Santos, E. A. Individual and combined effects of the elements Zn, Mg and Sr on the surface reactivity of a SiO2·CaO·Na2O·P2O5 bioglass system. *J. Non. Cryst. Solids* **2014**, *386*, 19–28, doi:10.1016/j.jnoncrysol.2013.11.038.

15.   Wang, X.; Li, X.; Ito, A.; Sogo, Y. Synthesis and characterization of hierarchically macroporous and mesoporous CaO-MO-SiO 2-P 2O 5 (M = Mg, Zn, Sr) bioactive glass scaffolds. *Acta Biomater.* **2011**, *7*, 3638–3644, doi:10.1016/j.actbio.2011.06.029.

16.   Saino, E.; Grandi, S.; Quartarone, E.; Maliardi, V.; Galli, D.; Bloise, N.; Fassina, L.; De Angelis, M. G. C.; Mustarelli, P.; Imbriani, M.; Visai, L. In vitro calcified matrix deposition by human osteoblasts onto a zinc-containing bioactive glass. *Eur. Cells Mater.* **2011**, *21*, 59–72, doi:10.22203/eCM.v021a05.

17.   Imani Fooladi, A. A.; Hosseini, H. M.; Hafezi, F.; Hosseinnejad, F.; Nourani, M. R. Sol-gel-derived bioactive glass containing SiO 2 -MgO-CaO-P 2 O 5 as an antibacterial scaffold. *J. Biomed. Mater. Res. Part A* **2013**, *101A*, 1582–1587, doi:10.1002/jbm.a.34464.

18.   Omar, S.; Repp, F.; Desimone, P. M.; Weinkamer, R.; Wagermaier, W.; Ceré, S.; Ballarre, J. Sol-gel hybrid coatings with strontium-doped 45S5 glass particles for enhancing the performance of stainless steel implants: Electrochemical, bioactive and in vivo response. *J. Non. Cryst. Solids* **2015**, *425*, 1–10, doi:10.1016/j.jnoncrysol.2015.05.024.

19. Lao, J.; Jallot, E.; Nedelec, J.-M. Strontium-Delivering Glasses with Enhanced Bioactivity: A New Biomaterial for Antiosteoporotic Applications? *Chem. Mater.* **2008**, *20*, 4969–4973.

20. Gentleman, E.; Fredholm, Y. C.; Jell, G.; Lotfibakhshaiesh, N.; O'Donnell, M. D.; Hill, R. G.; Stevens, M. M. The effects of strontium-substituted bioactive glasses on osteoblasts and osteoclasts in vitro. *Biomaterials* **2010**, *31*, 3949–3956, doi:10.1016/j.biomaterials.2010.01.121.

21. Dietrich, E.; Oudadesse, H.; Lucas-Girot, A.; Mami, M. In vitro bioactivity of melt-derived glass 46S6 doped with magnesium. *J. Biomed. Mater. Res. - Part A* **2009**, *88*, 1087–1096, doi:10.1002/jbm.a.31901.

22. Varanasi, V. G.; Saiz, E.; Loomer, P. M.; Ancheta, B.; Uritani, N.; Ho, S. P.; Tomsia, A. P.; Marshall, S. J.; Marshall, G. W. Enhanced osteocalcin expression by osteoblast-like cells (MC3T3-E1) exposed to bioactive coating glass (SiO2–CaO–P2O5–MgO–K2O–Na2O system) ions. *Acta Biomater.* **2009**, *5*, 3536–3547, doi:10.1016/j.actbio.2009.05.035.

23. Varmette, E. A.; Nowalk, J. R.; Flick, L. M.; Hall, M. M. Abrogation of the inflammatory response in LPS-stimulated RAW 264.7 murine macrophages by Zn- and Cu-doped bioactive sol-gel glasses. *J. Biomed. Mater. Res. - Part A* **2009**, *90*, 317–325, doi:10.1002/jbm.a.32098.

24. Karadjian, M.; Essers, C.; Tsitlakidis, S.; Reible, B.; Moghaddam, A.; Boccaccini, A.; Westhauser, F. Biological Properties of Calcium Phosphate Bioactive Glass Composite Bone Substitutes: Current Experimental Evidence. *Int. J. Mol. Sci.* 2019, *20*, 305.

25. Bellucci, D.; Sola, A.; Cannillo, V. Hydroxyapatite and tricalcium phosphate composites with bioactive glass as second phase: State of the art and current applications. *J. Biomed. Mater. Res. - Part A* **2016**, *104A*, 1030–1056, doi:10.1002/jbm.a.35619.

26. Bellucci, D.; Sola, A.; Gazzarri, M.; Chiellini, F.; Cannillo, V. A new hydroxyapatite-based biocomposite for bone replacement. *Mater. Sci. Eng. C* **2012**, *33*, 1091–1101, doi:10.1016/j.msec.2012.11.038.

27. Popa, A. C.; Stan, G. E.; Husanu, M. A.; Mercioniu, I.; Santos, L. F.; Fernandes, H. R.; Ferreira, J. M. F. Bioglass implant-coating interactions in synthetic physiological fluids with varying degrees of biomimicry. *Int. J. Nanomedicine* **2017**, *12*, 683–707, doi:10.2147/IJN.S123236.

28. Serra, J.; González, P.; Liste, S.; Serra, C.; Chiussi, S.; León, B.; Pérez-Amor, M.; Ylanen, H. O.; Hupa, M. FTIR and XPS studies of bioactive silica based glasses. *J. Non. Cryst. Solids* **2003**, *332*, 20–27, doi:10.1016/j.jnoncrysol.2003.09.013.

29. Raynaud, S.; Champion, E.; Bernache-Assollant, D.; Thomas, P. Calcium phosphate apatites with variable Ca/P atomic ratio I. Synthesis, characterisation and thermal stability of powders. *Biomaterials* **2002**, *23*, 1065–1072, doi:10.1016/S0142-9612(01)00218-6.

30. T. Kokubo, H. Takadama, How useful is SBF in predicting in vivo bone bioactivity?, Biomaterials. 27 (2006) 2907–2915. doi:10.1016/j.biomaterials.2006.01.017.

31. Rocha, J. H. G.; Lemos, A. F.; Agathopoulos, S.; Kannan, S.; Valério, P.; Ferreira, J. M. F. Hydrothermal growth of hydroxyapatite scaffolds from aragonitic cuttlefish bones. *J. Biomed. Mater. Res. - Part A* **2006**, *77*, 160–168, doi:10.1002/jbm.a.30566.

32. Goel, A.; Kapoor, S.; Tilocca, A.; Rajagopal, R. R.; Ferreira, J. M. F. Structural role of zinc in biodegradation of alkali-free bioactive glasses. *J. Mater. Chem. B* **2013**, *1*, 3073–3082, doi:10.1039/c3tb20163e.

33. Gerhardt, L.-C.; Boccaccini, A. R. Bioactive glass and glass-ceramic scaffolds for bone tissue engineering. *Materials (Basel).* **2010**, *3*, 3867–3910, doi:10.1016/B978-1-84569-768-6.50005-3.